Transmission probability through a Lévy glass and comparison with a Lévy walk

Groth, C.W.; Akhmerov, A.R.; Beenakker, C.W.J.

Transmission probability through a Lévy glass and comparison with a Lévy walk

C. W. Groth,[1,2] A. R. Akhmerov,[1] and C. W. J. Beenakker[1]
[1]*Instituut-Lorentz, Universiteit Leiden, P.O. Box 9506, NL-2300 RA Leiden, The Netherlands*
[2]*SPSMS, UMR-E 9001, CEA-INAC/UJF-Grenoble 1, F-38054 Grenoble, France*
(Received 20 May 2011; revised manuscript received 14 January 2012; published 23 February 2012)

Recent experiments on the propagation of light over a distance L through a random packing of spheres with a power-law distribution of radii (a so-called Lévy glass) have found that the transmission probability $T \propto 1/L^{\gamma}$ scales superdiffusively ($\gamma < 1$). The data has been interpreted in terms of a Lévy walk. We present computer simulations to demonstrate that diffusive scaling ($\gamma \approx 1$) can coexist with a divergent second moment of the step size distribution [$p(s) \propto 1/s^{1+\alpha}$ with $\alpha < 2$]. This finding is in accord with analytical predictions for the effect of step size correlations, but deviates from what one would expect for a Lévy walk of independent steps.

DOI: 10.1103/PhysRevE.85.021138 PACS number(s): 05.40.Fb, 05.60.Cd, 42.25.Bs, 42.25.Dd

I. INTRODUCTION

A random walk with a step size distribution that has a divergent second moment is called a Lévy walk [1–3]. A Lévy *glass* is a random medium where the separation between two scattering events has a divergent second moment. The term was coined by Barthelemy, Bertolotti, and Wiersma [4], for a random packing of polydisperse glass spheres. They measured the fraction T of the light intensity transmitted through such a random medium in a slab of thickness L, and found a power-law scaling $T \propto 1/L^{\gamma}$ with a superdiffusive exponent $\gamma \approx 0.5$—intermediate between the values for ballistic motion ($\gamma = 0$) and regular diffusion ($\gamma = 1$).

The simplest theoretical description of propagation through a Lévy glass neglects correlations between subsequent scattering events. The ray optics of the problem is then described by a Lévy walk, with a power-law step size distribution $p(s) \propto 1/s^{1+\alpha}$, $0 < \alpha < 2$. The experiment [4] was interpreted in these terms, with $\alpha = 1$ and $\gamma = \alpha/2$ the expected transmission exponent.

Correlations between scattering events in a Lévy glass dominate the dynamics in one dimension [5,6]. Although correlations were expected to become less significant with increasing dimensionality [7,8], Buonsante, Burioni, and Vezzani [9] have calculated that the transmission exponent γ should remain much larger than would follow from a Lévy walk with uncorrelated steps. In particular, a saturation at the diffusive value $\gamma = 1$ for $\alpha > 1$ is predicted—even though the second moment of the step size distribution becomes finite only for $\alpha > 2$.

To test these analytical predictions for the effect of correlations, we have simulated the transmission of classical particles through a Lévy glass, confined to a slab of thickness L. Both a two-dimensional (2D) system of disks is considered and a three-dimensional (3D) system of spheres. We find a power-law scaling $T(L) \propto 1/L^{\gamma}$ with an exponent γ that lies well above the $\gamma = \alpha/2$ line expected for a Lévy walk. In particular, we obtain a saturation of γ at the diffusive value of unity well before the $\alpha = 2$ threshold is reached of a divergent second moment.

The outline of the paper is as follows. Since our aim is to compare the Lévy glass simulations with the predictions for a Lévy walk, we need analytical results for uncorrelated step sizes. These are summarized in the Appendix and referred to in the main text. We start off in Sec. II with a description of the way in which we construct and simulate a Lévy glass on a computer. The results presented in that section are for 2D, where the largest systems can be studied. We turn to the 3D case in Sec. III and compare with the experiments [4]. We conclude in Sec. IV.

II. LÉVY GLASS VERSUS LÉVY WALK

A. Construction

A Lévy glass [4,10] is a random packing of transparent spheres with a power-law distribution of radii,

$$n(r) \propto 1/r^{1+\beta}. \tag{2.1}$$

Light propagates without scattering (ballistically) through the spheres and diffusively (mean free path $l_{\rm mfp}$) in the region between the spheres. The probability to enter a d-dimensional sphere of radius between r and $r + dr$ is proportional to the fraction $n(r)dr$ of spheres in that size range, multiplied by the area $\propto r^{d-1}$. The ballistic segments (steps) of a ray inside a sphere of radius r have length s of order r. The sphere radius distribution (2.1) therefore corresponds to the step size distribution [11]

$$p(s) \propto 1/s^{1+\alpha}, \quad \text{with} \quad \beta = \alpha + d - 1. \tag{2.2}$$

Particles propagating through a Lévy glass therefore have the same distribution of single step sizes as in a Lévy walk, but the joint distribution of multiple step sizes is different: while in a Lévy walk the steps are all uncorrelated (annealed disorder), in the Lévy glass the configuration of spheres is fixed so subsequent steps are correlated (quenched disorder).

We discuss in some details the construction of the 2D Lévy glass; see Fig. 1—the 3D version is entirely analogous. We start by generating disks of (dimensionless) radius

$$r_k = r_{\rm max}\left[1 + \frac{k}{k_{\rm max}}\left(r_{\rm max}^{\beta} - 1\right)\right]^{-1/\beta}, \qquad k = 0,1,2,\ldots,k_{\rm max}. \tag{2.3}$$

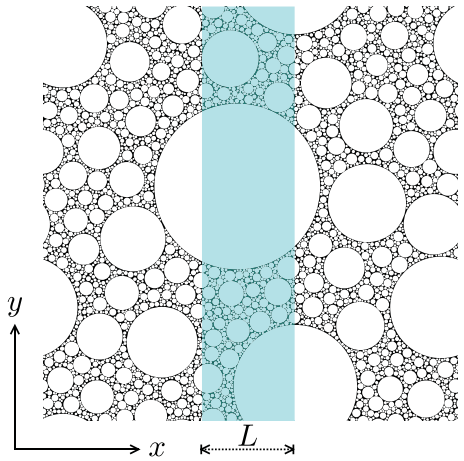

FIG. 1. (Color online) Two-dimensional Lévy glass, consisting of a random packing of disks with a power-law distribution of radii ($\alpha = 0.7$, $f = 0.86$, and $r_{\rm max}/r_{\rm min} = 100$). The blue shaded region defines a slab of thickness L. This is the unconstrained geometry, because the maximum disk size can be larger than L.

The $k_{\rm max}+1$ disks have radii ranging from $r_{\rm min} \equiv 1$ to $r_{\rm max} \gg 1$, and in this size range their distribution follows the power law (2.1). The average area of a disk is

$$\langle A\rangle = \frac{\pi\beta}{|2-\beta|}\max\left(1, r_{\rm max}^{2-\beta}\right). \tag{2.4}$$

The entire Lévy glass occupies an area of dimension $W \times W$ in the x-y plane, with periodic boundary conditions and W about 10–100 times larger than $r_{\rm max}$. For a random packing, we place the disks at randomly chosen positions in the order $k = 0,1,2,\ldots$ (so starting from the largest disk). If disk number k overlaps with any of the disks already in place, another random position is attempted. For each disk, some 10^4 attempted placements are made. If they are all unsuccessful, the entire construction is started over with a smaller value of $k_{\rm max}$.

The density of the packing is quantified by the filling fraction

$$f = k_{\rm max}\langle A\rangle/W^2. \tag{2.5}$$

For each simulation, we strove for maximal f by maximizing $k_{\rm max}$. The maximal filling fraction increases with increasing ratio $r_{\rm max}/r_{\rm min}$, as illustrated in Fig. 2. For the smallest α, below about 0.4, we could not reach as dense a packing as for larger α, basically because there are too few small disks. Somewhat larger filling fractions would be reachable by moving the disks after placement, but we did not attempt that.

B. Dynamics

The ballistic dynamics inside the spheres consists of chords of varying length s traversed in a time s/v. The diffusive dynamics in between the spheres is modeled by a Poisson process: isotropic scattering in a time interval dt with probability $v\,dt/l_{\rm mfp}$. The mean free path $l_{\rm mfp} = r_{\rm min}/2$ is chosen such that there is, on average, one scattering event between leaving and entering a sphere. We take the same refractive index (and velocity v) inside and outside the spheres, so the ray is not refracted at the interface.

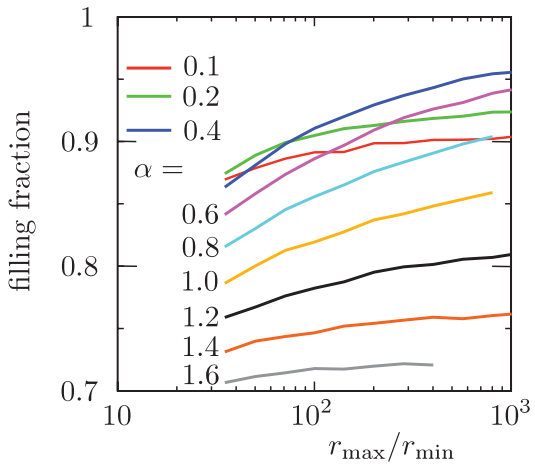

FIG. 2. (Color online) Filling fraction of the 2D Lévy glass as a function of the ratio $r_{\rm max}/r_{\rm min}$ of largest and smallest disk size, for several values of the parameter α.

In Fig. 3, we show the step size distribution $p(s)$ for a 2D Lévy glass with disk radius distribution (2.1), for $\beta = 2.2$. It follows closely the Lévy distribution (2.2), with the expected parameter value $\alpha = \beta - 1 = 1.2$ (solid line).

We do not find the pronounced oscillations in $p(s)$, which in Ref. [10] complicated the determination of α. These oscillations appear due to coarse graining of the disk size distribution $n(r)$ and vanish if a finer distribution of disk sizes is used.

The time dependence of the mean-squared displacement $\langle \Delta r(t)^2\rangle$ is shown in Fig. 4, for the same $\alpha = 1.2$. A particle was started at a random position $\boldsymbol{r}(0)$ in the interdisk region, and then its position $\boldsymbol{r}(t)$ at time t (either inside or outside a disk) gives the displacement $\Delta r(t) = |\boldsymbol{r}(t) - \boldsymbol{r}(0)|$. The average $\langle\cdots\rangle$ is over some 10^4 initial positions. In accord with previous simulations [4,10], regular (Brownian) diffusion with $\langle \Delta r(t)^2\rangle \propto t$ is reached for times $t \gtrsim r_{\rm max}/v \equiv t_{\rm D}$, set by the time needed to traverse the largest disk. For $t < t_{\rm D}$,

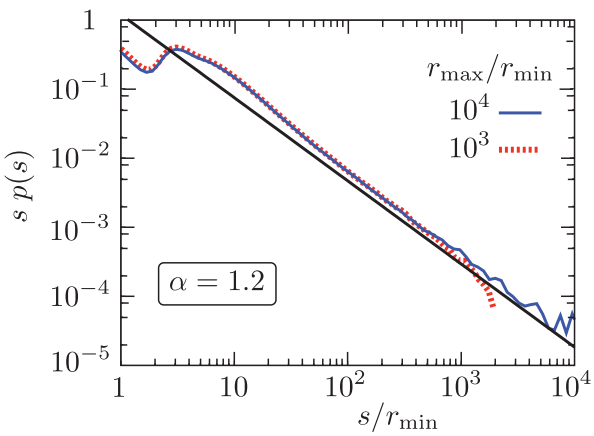

FIG. 3. (Color online) Step size distribution for a random packing of disks with radius distribution (2.1) (for $\beta = 2.2$, so $\alpha = 1.2$). The numerical results are shown for two values of the maximum disk radius ($r_{\rm max}/r_{\rm min} = 10^4$ and 10^3, with $f = 0.83$ and 0.80, respectively). The black solid line is the expected distribution (2.1).

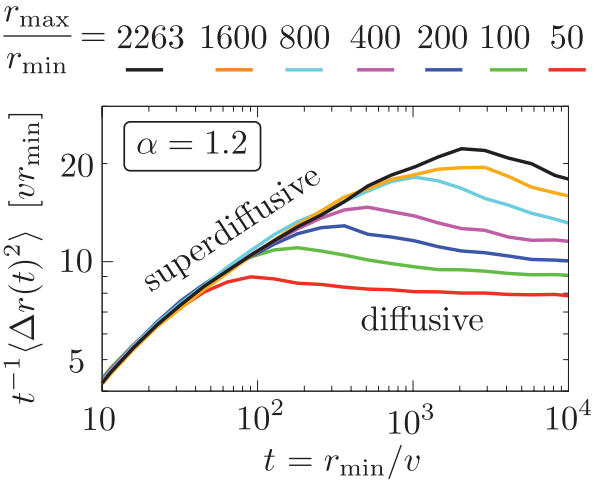

FIG. 4. (Color online) Time dependence of the mean-square displacement (divided by t so that saturation indicates diffusive scaling). The curves are the results of a numerical simulation in a 2D Lévy glass with different values of $r_{\max}/r_{\min}$, at fixed $\alpha = 1.2$. The ratio $r_{\max}/r_{\min}$ decreases from top to bottom.

the mean-squared displacement increases more rapidly than linearly (superdiffusion).

The limiting slope of the mean-square displacement for $t \gg t_D$ gives the diffusion constant in the Brownian regime,

$$D = \lim_{t\to\infty} \frac{1}{2\,dt} \langle \Delta r(t)^2 \rangle. \tag{2.6}$$

As shown in Fig. 5, this diffusion constant has a power-law dependence on $r_{\max}$,

$$D(r_{\max}) \propto r_{\max}^{1-\gamma_D}, \tag{2.7}$$

with $0 < \gamma_D < 1$. (For the smallest $\alpha = 0.2$, no clear power-law scaling was observed.)

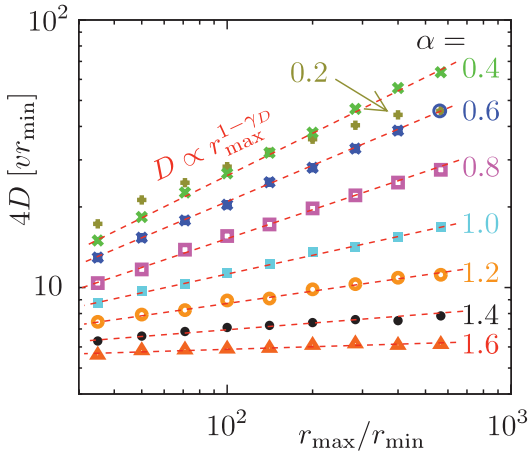

FIG. 5. (Color online) Diffusion coefficient (2.6) in the Brownian regime, estimated from the large-t slope of the mean-square displacement (corresponding to the large-t saturation value in Fig. 4). Each set of colored data points represents one value of α, with different values of $r_{\max}/r_{\min}$. The power-law scaling (2.7) (red dotted lines) determines the scaling exponent γ_D.

C. Transmission probability

For the transmission problem, we need a slab of variable thickness L. We distinguish two ways of constructing this geometry. One way is to obtain the slab from the entire Lévy glass by cutting out the region $0 < x < L$ (blue strip in Fig. 1). We call this an unconstrained geometry, because $r_{\max}$ is not constrained to be smaller than L. The alternative constrained geometry (used in the experiments [4]) requires that the spheres all lie fully inside the slab, thereby restricting $r_{\max} < L/2$. We consider the transmission probabilities in the unconstrained and constrained geometries in separate subsections, both for 2D. (Results for 3D are presented in the next section.)

D. Unconstrained geometry

A lower limit $T_{\rm ball}$ to the transmission probability $T_{\rm uncon}$ in the unconstrained geometry follows by considering only ballistic rays, which pass through the region $0 < x < L$ without a single scattering event. As explained in the Appendix, see Eq. (A7), this probability is directly related to the step size distribution,

$$T_{\rm ball} = \frac{1}{\langle s \rangle} \int_L^\infty dx \int_x^\infty ds\, p(s). \tag{2.8}$$

We take the step size distribution (2.2) with an upper cutoff at $s_{\max} \simeq r_{\max} \gg L$ and a lower cutoff at $s_{\min} \simeq 1$. Then Eq. (2.8) evaluates to

$$T_{\rm ball} \simeq \frac{r_{\max} - \alpha^{-1} L^{1-\alpha} r_{\max}^{\alpha}}{r_{\max} - r_{\max}^{\alpha}}$$
$$\to r_{\max} \gg L \begin{cases} 1 & \text{for} \quad 0 < \alpha < 1, \\ L^{1-\alpha} & \text{for} \quad 1 < \alpha < 2. \end{cases} \tag{2.9}$$

Since $T_{\rm ball} \leqslant T_{\rm uncon} \leqslant 1$, we can immediately conclude that $T_{\rm uncon} = 1$ for $0 < \alpha < 1$. For $1 < \alpha < 2$, the power-law scaling $T_{\rm uncon} \propto 1/L^{\gamma}$ must satisfy $\gamma \leqslant \alpha - 1$. This holds irrespective of correlations between multiple steps, since these cannot affect $T_{\rm ball}$. If we neglect these correlations, we may equate $T_{\rm uncon}$ to the transmission probability $T_{\rm eq}$ of a Lévy walk with equilibrium initial conditions (see Appendix A3). In view of Eq. (A9), this leads to $\gamma = \alpha - 1$. We believe this result to be quite robust, since even if correlations do play a role, it is likely that they slow down the superdiffusion [7,8], so they would not lead to a smaller γ.

In Fig. 6, we show the L dependence of $T_{\rm uncon}$ for two values of α, resulting from a numerical simulation of an unconstrained 2D Lévy glass. This is data up to $r_{\max} = 10^4$ for $\alpha = 1.1$ and up to $r_{\max} = 10^3$ for $\alpha = 1.5$, which is at the upper limit of our computational resources. As expected from the Lévy walk (Fig. 13), the convergence to the $r_{\max} \to \infty$ limit is very slow, and we are not able to conclusively test the predicted asymptote.

E. Constrained geometry

For the construction of a constrained Lévy glass, we limited the maximum disk radius to $r_{\max} = L/4$ and ensured that all disks fit inside the slab of thickness L. The corresponding random walk would be a truncated Lévy walk with maximum

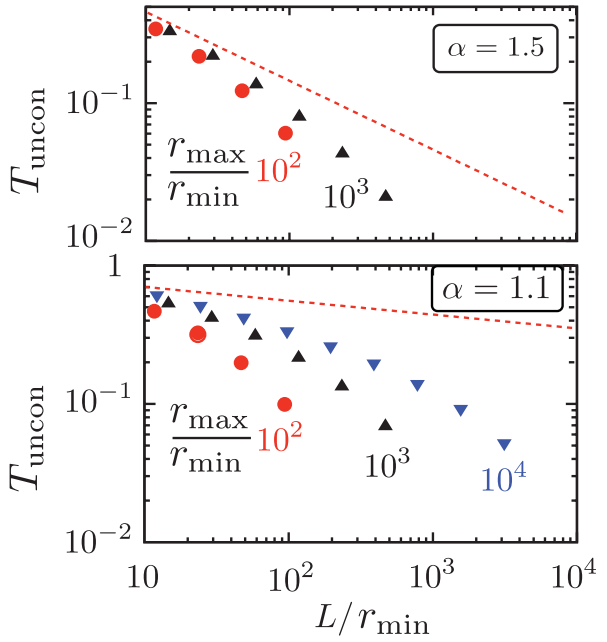

FIG. 6. (Color online) Transmission probability $T_{\rm uncon}$ through a 2D *unconstrained* Lévy glass, for different values of the maximum disk radius $r_{\rm max}$. The dotted line is the predicted scaling $T_{\rm uncon} \propto L^{1-\alpha}$ in the $r_{\rm max} \to \infty$ limit.

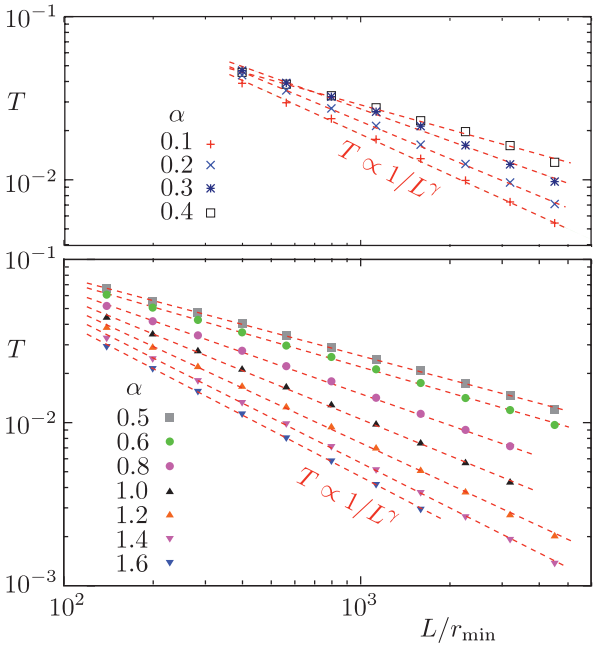

FIG. 7. (Color online) Transmission probability through a 2D constrained Lévy glass as a function of the thickness of the slab, for different values of the step size exponent α. The dotted lines are a linear fit to the data points, determining the transmission scaling exponent γ. (The data is split over two panels, to avoid overlap.)

step size $s_{\rm max} \simeq L/2$. From the analysis in Appendix 4b we would therefore expect a $T \propto 1/L^{\alpha/2}$ scaling of the transmission probability—if correlations between step sizes would not matter.

In Fig. 7, we show the scaling of the transmission probability,

$$T \propto 1/L^{\gamma}, \tag{2.10}$$

as it follows from the simulation. The power-law scaling applies to somewhat less than two decades in L for $\alpha \gtrsim 0.5$ (lower panel), and to one decade for smaller α (upper panel). In Fig. 8, we give the resulting exponent γ as a function of α.

In the same figure, we show the scaling of the diffusion exponent γ_D, from Eq. (2.7). (There we could only obtain a power-law scaling for $\alpha \gtrsim 0.4$.) As expected from the identification of $T \simeq D(L)/L \propto 1/L^{\gamma_D}$, one has in good approximation

$$\gamma = \gamma_D. \tag{2.11}$$

III. COMPARISON WITH EXPERIMENTS

The numerical data shown so far was for a 2D Lévy glass of disks. We have also performed simulations for a 3D Lévy glass of spheres, in the constrained geometry with $r_{\rm max} = L/4$. We went up to $L/r_{\rm min} = 1132$ for $\alpha \leqslant 0.8$ and up to $L/r_{\rm min} = 800$ for $\alpha = 1$ and 1.2. (Larger values of α could not be simulated reliably.) Although the systems are smaller in 3D than in 2D, the results are quite similar; see the comparison in Fig. 9 of the α dependence of the transmission exponent γ for a 2D and a 3D Lévy glass. In particular, for both 2D and 3D, the results for γ lie well above the $\gamma = \alpha/2$ line.

We can now compare directly with the 3D experiments [4], which obtained $\gamma = 0.5$ within experimental accuracy for $\alpha = 1$. Our simulation, in contrast, gives for $\alpha = 1$ a value for γ that is about 50% higher. We cannot attribute the difference to finite-size effects, since the 3D simulation reaches the same range of system sizes as the experiment. There are aspects of the experiment that are not present in the simulation (notably absorption), but we believe that the difference is mainly due to an irregularity in the experimental sphere size distribution.

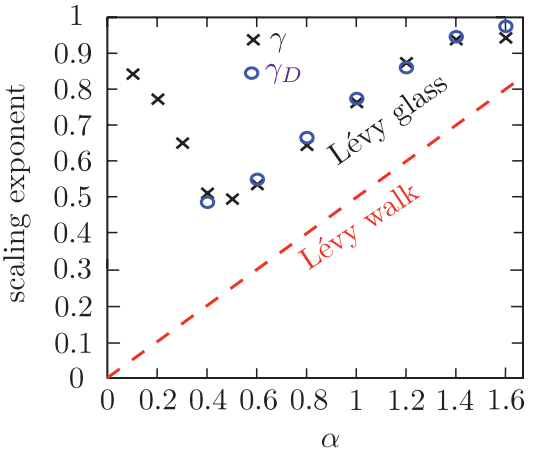

FIG. 8. (Color online) Exponents γ and γ_D, governing the scaling of the transmission probability (2.10) (crosses) and diffusion constant (2.7) (circles). These are the results of a simulation of a 2D constrained Lévy glass (see Figs. 5 and 7). The red dashed line is the prediction (A20) for a Lévy walk with nonequilibrium initial conditions.

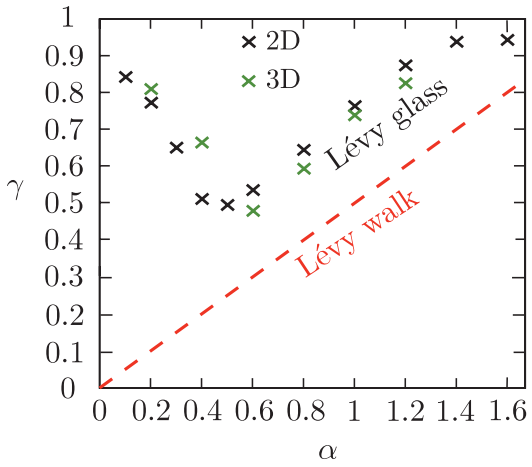

FIG. 9. (Color online) Comparison of the α dependence of the transmission exponent γ for a 2D and 3D Lévy glass. Both data sets lie well above the $\gamma = \alpha/2$ line of a Lévy walk.

To visualize the irregularity, we plot in Fig. 10 the quantity

$$V(r) = \frac{4}{3}\pi \int_r^\infty r'^3 n(r')dr', \tag{3.1}$$

which is the cumulative volume enclosed by spheres with radii greater than r. This is a decreasing function of r, from $V(r_{\min}) = V_0$ (the total sphere volume) down to $V(r_{\max}) = 0$. For the Lévy distribution with $\alpha = 1$ in 3D we have $n(r) \propto r^{-4}$, cf. Eqs. (2.1) and (2.2); hence $V(r)$ should decrease linearly as a function of $\log r$,

$$V(r) = -\frac{V_0}{\log(r_{\max}/r_{\min})} \log(r/r_{\max}). \tag{3.2}$$

As shown in Fig. 10, the experimental sphere size distribution differs markedly from the expected Lévy form (3.2). Rather than a single linear dependence of $V(r)$ on $\log r$, there are two piecewise linear dependencies with a different slope, joined with a kink at $r \approx 50\,\mu$m. This irregularity has the effect of reducing the transmission exponent γ, essentially by mimicking a system with a smaller value of α.

To demonstrate the effect of the kink on the transmission exponent, we have simulated the experiment by constructing

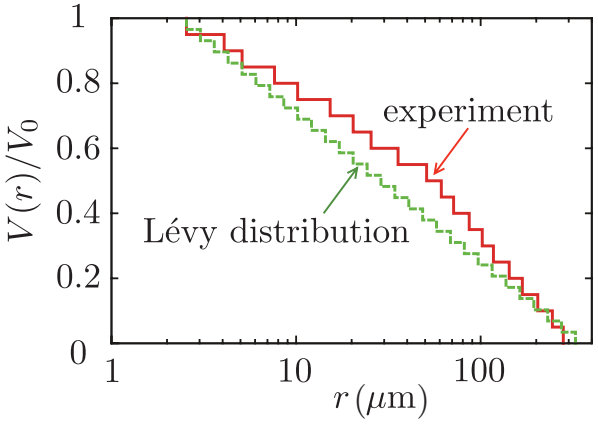

FIG. 10. (Color online) Sphere volume distribution used in the experiment [4] (red solid histogram) and for an $\alpha = 1$ Lévy distribution (green dashed histogram).

a random packing of spheres with the experimental size distribution (red solid histogram in Fig. 10). All spheres were constrained to fit inside a slab of thickness L. (We took $r_{\max} = L/2.1$ for this simulation.) We found $\gamma = 0.57$. If, instead, we used the proper Lévy size distribution (green dashed histogram), keeping all other parameters the same, we found $\gamma = 0.72$. We believe this resolves the issue.

IV. CONCLUSION

In conclusion, we have found that the superdiffusive scaling $T \propto 1/L^\gamma$ of the transmission probability through a Lévy glass, constrained to a slab of thickness L, deviates substantially from what one would expect for a Lévy walk. Most significantly, the diffusive scaling ($\gamma \approx 1$) can coexist with a divergent second moment of the step size distribution ($\alpha < 2$).

As a consistency check on our simulations, we have also calculated the diffusion constant D from the long-time limit of the mean square displacement in an unbounded Lévy glass, as a function of the maximum disk size $r_{\max}$. We find $D(r_{\max}) \propto r_{\max}^{1-\gamma_D}$, with $\gamma_D \approx \gamma$, as expected for a diffusive transmission probability $T \simeq D(L)/L$ with a scale-dependent diffusion constant.

Qualitatively, our finding that diffusive scaling of T can coexist with a divergent second moment of $p(s)$ is consistent with analytical calculations for $d = 1$ [5] and $d = 2,3$ [9]. Quantitatively, we are not in agreement: Ref. [9] finds that γ increases monotonically for $d = 2$ from $\gamma = 0$ at $\alpha = 0$ to $\gamma = 1$ for $\alpha \geqslant 1$, while our simulation gives a nonmonotonic α dependence of γ, with a saturation for $\alpha \gtrsim 1.5$ (see Fig. 8). The system considered in Ref. [9] is quasiperiodic (a Lévy quasicrystal), rather than the random Lévy glass studied here. Further study is needed to see whether this difference is at the origin of the different transmission scaling, or whether the difference is due to a very slow convergence to the infinite system-size limit (which we consider more likely).

ACKNOWLEDGMENTS

This research was supported by the Dutch Science Foundation NWO/FOM.

APPENDIX: TRANSMISSION PROBABILITY OF A LÉVY WALK

1. Formulation of the problem

We consider a random walk along the x axis with the power-law step size distribution

$$p(s) = \frac{\alpha}{s_0}\left(\frac{s_0}{s}\right)^{1+\alpha} \theta(s - s_0). \tag{A1}$$

[The function $\theta(s - s_0)$ equals 1 if $s > s_0$ and 0 if $s < s_0$.] Subsequent steps are $+s$ or $-s$ with equal probability and independently distributed. The probability density $p(s)$ decays as $1/s^{1+\alpha}$ with $\alpha > 0$, starting from a minimal step size $s_0 > 0$. In between two scattering events the walker has a constant velocity of magnitude v. This random walk is called Brownian or diffusive for $\alpha > 2$, Lévy [3] or superdiffusive for $1 < \alpha < 2$, and quasiballistic for $0 < \alpha < 1$.

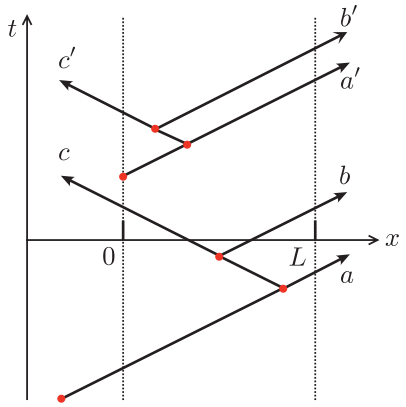

FIG. 11. (Color online) Trajectories $x(t)$ of a random walk, with scattering events indicated by red dots. All trajectories enter the segment $0 < x < L$ (between dotted lines) at $x = 0$. Trajectories a,b,a',b' are transmitted through $x = L$, while trajectories c,c' are reflected through $x = 0$. The transmission probability $T_{\rm eq}$ averages over all trajectories (equilibrium initial conditions), while $T_{\rm noneq}$ averages only over trajectories such as a',b',c' that have a scattering event upon entering the segment at $x = 0$ (nonequilibrium initial conditions).

The walker enters the segment $0 < x < L$ by passing through $x = 0$ at time t_i and then stays in that segment until time t_f. If at t_f it exits through $x = L$, we say the walker has been transmitted through the segment. We seek the dependence of the transmission probability T on the length L of the segment, for $L \gg l_0$. For a Brownian walk, the scaling is inverse linear: $T \propto 1/L$ if $\alpha > 2$. For a Lévy walk, we expect a slower power-law decay, $T \propto 1/L^{\gamma}$ with $\gamma < 1$. The question is how γ varies with $\alpha < 2$.

The answer depends on how the walker is started off initially. Following Barkai, Fleurov, and Klafter [12], we distinguish equilibrium from nonequilibrium initial conditions. (See Fig. 11.) For equilibrium initial conditions, the walker starts off from $x = -\infty$, so that it crosses $x = 0$ at some random time between two scattering events. For nonequilibrium initial conditions, the walker starts off from $x = 0$ with a scattering event. We denote the transmission probabilities in these two cases by $T_{\rm eq}$ and $T_{\rm noneq}$, respectively, and consider the two cases in separate subsections.

2. Nonequilibrium initial conditions

The transmission probability $T_{\rm noneq}$ from $x = 0$ to $x = L$ for a Lévy walk that starts off with a scattering event at $x = 0$ has been calculated by several authors [13–15]. We give the most general solution of Buldyrev *et al.* [15].

They assume that the walker starts with a scattering event at an arbitrary point x_i in the segment $(0,L)$ and calculate the probability $P(x_i)$ that the walker exits the segment through $x = L$. For $L \gg s_0$ and $x_i \gg s_0$, their solution [15] can be written in the compact form

$$P(x_i) = \frac{B(x_i/L,\alpha/2,\alpha/2)}{B(1,\alpha/2,\alpha/2)}, \tag{A2}$$

in terms of the incomplete beta function

$$B(x,a,b) = \int_0^x y^{a-1}(1-y)^{b-1}dy. \tag{A3}$$

Since $B(x,a,b) \to x^a/a$ for $x \to 0$, one arrives at the scaling $T_{\rm noneq} \propto L^{-\alpha/2}$, first obtained by Davis and Marshak from basic considerations [13].

The prefactor of the power-law scaling cannot be obtained directly from the solution (A2), because of the limitation that $x_i \gg s_0$. For $0 < \alpha < 1$, we can work around this limitation by considering the first step separately. The walker starts off at $x = 0$ with a step to $x_1 > 0$, chosen randomly from the distribution (A1) of a Lévy walk. If $x_1 > L$, the walker is transmitted with unit probability. Otherwise, it is transmitted with probability $P(x_1)$.

We thus can calculate $T_{\rm noneq}$ from

$$T_{\rm noneq} = \int_L^\infty dx_1\, p(x_1) + \int_0^L dx_1\, p(x_1)P(x_1). \tag{A4}$$

For $\alpha < 1$, the mean step size diverges, so the region $x_1 \lesssim s_0$ is insignificant and we can use Eq. (A2) for $P(x_1)$. The result is

$$\begin{aligned} T_{\rm noneq} &= \frac{B(s_0/L,\alpha/2,1+\alpha/2)}{B(1,\alpha/2,1+\alpha/2)} \\ &\overset{L\gg s_0}{\to} \left(\frac{s_0}{L}\right)^{\alpha/2} \frac{4\Gamma(\alpha)}{\alpha\Gamma^2(\alpha/2)}. \end{aligned} \tag{A5}$$

While the exponent $\alpha/2$ holds for any $0 < \alpha < 2$, the prefactor is accurate only for $0 < \alpha < 1$. [For $\alpha > 1$, we would need to know $P(x_1)$ within the region $x_1 \lesssim s_0$ in order to calculate the prefactor.]

3. Equilibrium initial conditions

For equilibrium initial conditions, the walker crosses $x = 0$ at a random time between scattering events. The first subsequent scattering event is at a point $x_1 > 0$, with probability density $q(x_1)$. If $x_1 > L$, the walker is transmitted with unit probability; if $0 < x_1 < L$, the transmission probability is $P(x_1)$. Hence

$$T_{\rm eq} = \int_L^\infty dx_1 q(x_1) + \int_0^L dx_1 q(x_1)P(x_1). \tag{A6}$$

The probability density $q(x)$ is determined from the step size distribution,

$$q(x) = \frac{1}{\langle s\rangle}\int_x^\infty p(s)ds. \tag{A7}$$

This relation between the distribution $p(s)$ of the distance s between subsequent scattering events and the distribution $q(x)$ of the distance x from an arbitrary point to the next scattering event holds for any random walk with a finite average step size $\langle s\rangle = \int_0^\infty sp(s)ds$. For the step size distribution (A1), one has

$$q(x) = \frac{\alpha-1}{\alpha s_0}\left(\frac{s_0}{\max(x,s_0)}\right)^{\alpha}, \quad \text{for} \quad \alpha > 1. \tag{A8}$$

As emphasized in Ref. [12], the distribution $q(x) \propto 1/x^{\alpha}$ decays more slowly than the distribution $p(s) \propto 1/s^{1+\alpha}$ because the walker is more likely to cross $x = 0$ during a

long step than during a short step, so long steps carry more weight in $q(x)$ than they do in $p(s)$. Indeed, for $1 < \alpha < 2$, the first moment of $q(x)$ is infinite, while the first moment of $p(s)$ is finite.

Substitution of Eqs. (A2) and (A8) into Eq. (A6) gives, for $L \gg s_0$,

$$T_{\rm eq} = \left(\frac{s_0}{L}\right)^{\alpha-1} \frac{\pi\Gamma(\alpha)}{\alpha \sin(\alpha\pi/2)\Gamma^2(\alpha/2)}, \quad \text{for} \quad 1 < \alpha < 2. \tag{A9}$$

This scaling $T_{\rm eq} \propto 1/L^{\alpha-1}$ holds in the superdiffusive regime $1 < \alpha < 2$. In the quasiballistic regime, the first scattering event is at $x_1 > L$ with unit probability,

$$T_{\rm eq} = 1, \quad \text{for} \quad 0 < \alpha \leqslant 1. \tag{A10}$$

The value $\alpha = 2$ at the border between a Brownian walk and a Lévy walk requires separate consideration. While $T_{\rm noneq} \propto 1/L$ for $\alpha = 2$, the transmission probability (A6) has a logarithmic enhancement,

$$T_{\rm eq} = \frac{s_0}{L}\left(1 + \frac{1}{2}\ln\frac{L}{s_0}\right), \quad \text{for} \quad \alpha = 2. \tag{A11}$$

A similar but different scaling $\propto L^{-1}\sqrt{\ln L}$ has been associated with the $\alpha = 2$ Lévy walk in Ref. [14].

4. Truncated Lévy walk

A *truncated* Lévy walk has step size distribution

$$p_{\rm trunc}(s) = \frac{\alpha}{s_0}\left(\frac{s_0}{s}\right)^{1+\alpha} \theta(s - s_0)\theta(s_{\rm max} - s), \tag{A12}$$

with a maximum step size $s_{\rm max} \gg s_0$. The root-mean-squared displacement σ after a single step then has a finite value,

$$\sigma = \sqrt{\frac{\alpha}{2-\alpha}}\, s_{\rm max}^{1-\alpha/2} s_0^{\alpha/2}, \tag{A13}$$

much smaller than $s_{\rm max}$ for $\alpha < 2$.

The transition from a truncated Lévy walk to a Brownian walk requires $n_{\rm steps} \gg 1$ of steps, given by Refs. [16,17]

$$n_{\rm steps} \simeq \frac{(2-\alpha)^3}{\alpha}(s_{\rm max}/s_0)^{\alpha}. \tag{A14}$$

The corresponding root-mean-squared displacement $\sigma\sqrt{n_{\rm steps}} \simeq (2-\alpha)s_{\rm max}$ is of order $s_{\rm max}$ for all $\alpha < 2$. We conclude that we have regular (Brownian) diffusion over a distance L if $s_{\rm max} \lesssim L$.

The transmission probability $P(x)$ for a walker starting with a scattering event at a point x inside a slab of thickness L (further than $s_{\rm max}$ from the boundaries) thus follows the usual diffusive scaling,

$$P(x) = x/L, \quad \text{if} \quad x, L - x \gtrsim s_{\rm max}. \tag{A15}$$

a. Equilibrium initial conditions

For equilibrium initial conditions, the distribution $q(x)$ of the first scattering event follows from Eq. (A7), with p replaced by $p_{\rm trunc}$. Substitution into Eq. (A6) then determines the transmission probability (for $L > s_{\rm max}$),

$$T_{\rm eq} = \int_0^{s_{\rm max}} dx\, q(x)P(x). \tag{A16}$$

Equation (A15) gives $P(x)$ only for $x \gtrsim s_{\rm max}$. We will use this expression also for $x < s_{\rm max}$, and then test the approximation by comparing with numerical simulations in Sec. V.

If we substitute $P(x) = x/L$, we find

$$T_{\rm eq} = \frac{1}{2L}\,\frac{1-\alpha}{2-\alpha}\,\frac{s_{\rm max}^2 - s_{\rm max}^{\alpha} s_0^{2-\alpha}}{s_{\rm max} - s_{\rm max}^{\alpha} s_0^{1-\alpha}}, \tag{A17}$$

for $0 < \alpha < 1$ or $1 < \alpha < 2$. For $\alpha = 1$ or $\alpha = 2$, there are logarithmic factors,

$$T_{\rm eq} = \frac{s_{\rm max} - s_0}{2L\ln(s_{\rm max}/s_0)}, \quad \text{for} \quad \alpha = 1, \tag{A18a}$$

$$T_{\rm eq} = \frac{s_0}{2L}\,\frac{s_{\rm max}\ln(s_{\rm max}/s_0)}{s_{\rm max} - s_0}, \quad \text{for} \quad \alpha = 2. \tag{A18b}$$

For fixed $s_{\rm max}$, the diffusive $1/L$ scaling holds. An anomalous scaling appears if the maximum step size $s_{\rm max} = cL$ is a fixed fraction $c < 1$ of the slab thickness. Then the transmission probability through the slab depends on $L \gg s_0$ as

$$T_{\rm eq} = \frac{1}{2}c^{2-\alpha}\left(\frac{s_0}{L}\right)^{\alpha-1}\frac{\alpha-1}{2-\alpha}, \quad \text{for} \quad 1 < \alpha < 2, \tag{A19a}$$

$$T_{\rm eq} = \frac{1}{2}c\,\frac{1-\alpha}{2-\alpha}, \quad \text{for} \quad \alpha < 1, \tag{A19b}$$

$$T_{\rm eq} = \frac{c}{2\ln(cL/s_0)}, \quad \text{for} \quad \alpha = 1, \tag{A19c}$$

$$T_{\rm eq} = \frac{s_0\ln(cL/s_0)}{2L}, \quad \text{for} \quad \alpha = 2. \tag{A19d}$$

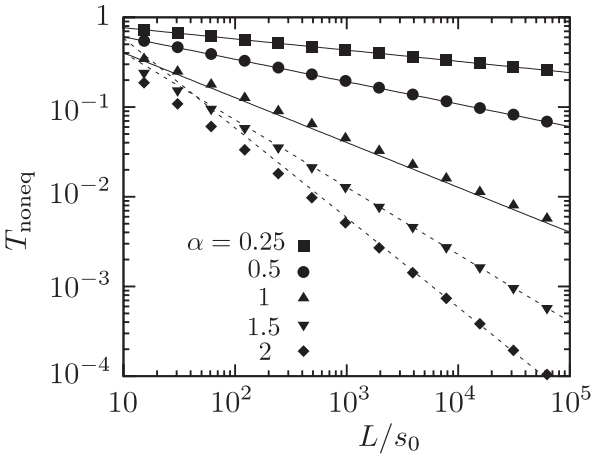

FIG. 12. Transmission probability $T_{\rm noneq}$ of a Lévy walk through a slab of thickness L, for *nonequilibrium* initial conditions. The data points are the results of a numerical simulation, for different values of the step size exponent α (and fixed $s_{\rm max} \gg L$). The lines indicate the expected $L^{-\alpha/2}$ scaling. For $\alpha < 1$, we also have an analytical prediction (A5) for the prefactor (solid lines), while for $\alpha > 1$ only the exponent is known analytically so the prefactor has been fitted to the data (dotted lines).

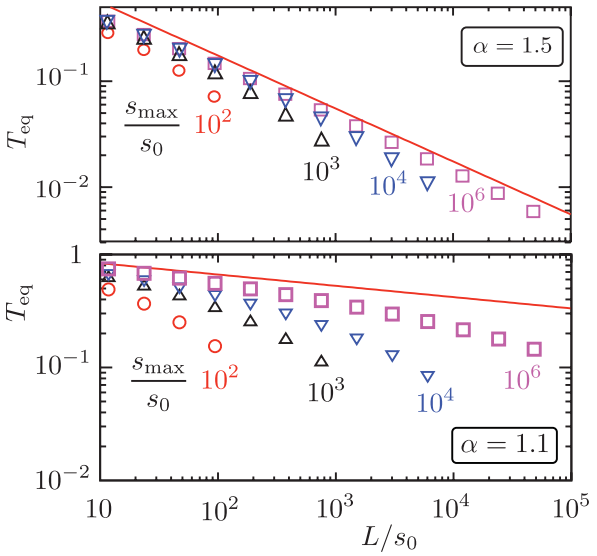

FIG. 13. (Color online) Transmission probability $T_{\rm eq}$ of a Lévy walk through a slab of thickness L, for *equilibrium* initial conditions. The two panels are for different values of α. The data points result from a numerical simulation, with different values $s_{\rm max}$ of the maximum step size. The solid line is the asymptote (A9) for $s_{\rm max} \to \infty$.

Hence $T_{\rm eq} \propto 1/L^{\max(0,\alpha-1)}$ (with logarithmic corrections for $\alpha = 1$ and $\alpha = 2$). This is the same scaling as for the Lévy walk without truncation (see Sec. III).

b. Nonequilibrium initial conditions

For nonequilibrium initial conditions, the transition to the regular diffusive regime happens while the walker is inside the slab. We may therefore assume that the usual diffusive scaling $T_{\rm noneq} \simeq \sigma/L$ applies (with σ playing the role of the mean free path). In view of Eq. (A13), an anomalous scaling appears if $s_{\rm max} = cL$ scales proportionally to L,

$$T_{\rm noneq} \simeq (cL)^{1-\alpha/2} s_0^{\alpha/2} L^{-1} \propto L^{-\alpha/2}. \qquad \text{(A20)}$$

The anomalous $L^{-\alpha/2}$ scaling of Appendix A2 now appears as a consequence of regular diffusion with a scale-dependent mean free path.

5. Numerical test

We have tested the analytical expressions (A5) and (A9) by numerical simulation. Results for $T_{\rm noneq}$ are shown in Fig. 12. This is the nonequilibrium initial condition, where the walker starts off at $x = 0$ with a step to positive x. The $L^{-\alpha/2}$ scaling is reproduced for all $0 < \alpha < 2$, and the prefactor (A5) agrees well with the simulations for $0 < \alpha \leqslant 1$.

For the equilibrium initial condition, the walker starts off at a large distance from $x = 0$, crossing the boundary at a random point between two scattering events. Results of numerical simulations are shown in Fig. 13. Unlike in the nonequilibrium case, the convergence to the asymptotic scaling with increasing $s_{\rm max}$ is very slow, in particular for small α.

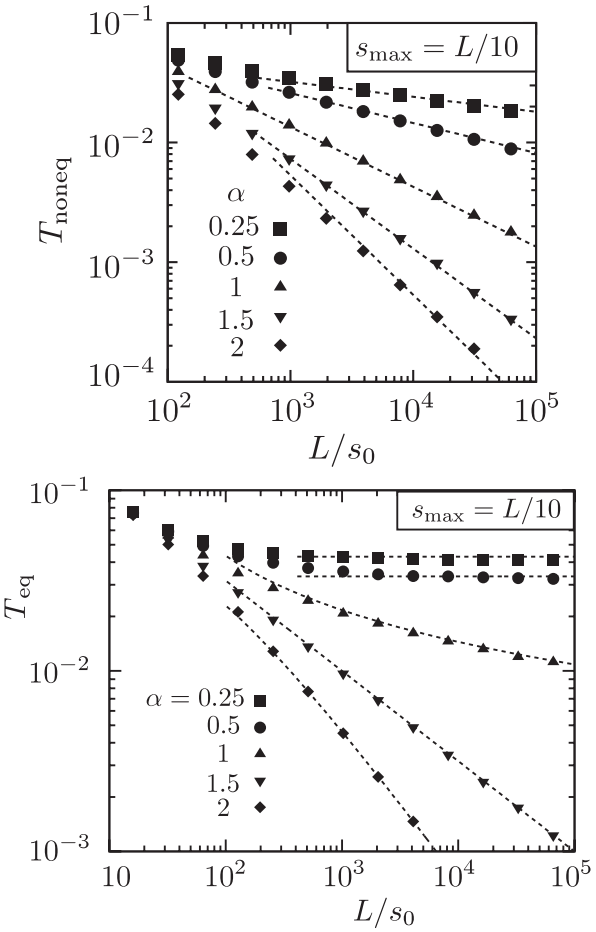

FIG. 14. Transmission probability for a Lévy walk with maximum step size $s_{\rm max}$ that increases proportionally to L. The two panels (both for $s_{\rm max} = L/10$) correspond to equilibrium and nonequilibrium initial conditions. The dotted lines show the expected scaling (A19) and (A20), up to a prefactor that has been fitted to the data. [For $T_{\rm eq}$ the difference with Eq. (A19) is a factor of 2, independent of α.]

We have also tested the scaling (A19) and (A20) for a truncated Lévy walk with a maximum step size $s_{\rm max}$ that is a fixed fraction of L. Results are shown in Fig. 14 for both equilibrium and nonequilibrium initial conditions. The anomalous scaling now appears, even though the diffusion is regular on the scale of L, because of the scale dependence of the mean free path. For both types of initial conditions the numerics follows closely the analytically predicted power laws, including the logarithmic factors for $\alpha = 1,2$ in the equilibrium case. (The constant prefactors are not given reliably by the analytics.)

[1] *Lévy Flights and Related Topics in Physics*, edited by M. Shlesinger, G. Zaslavsky, and U. Frisch (Springer, Berlin, 1995).

[2] R. Metzler and J. Klafter, Phys. Rep. **339**, 1 (2000).

[3] The difference between a Lévy walk and a Lévy flight is that in the walk the steps have a duration proportional to their length, while in the flight the steps are assumed to occur instantaneously. For the transmission probability the difference does not matter, but for the mean-square displacement it does.

[4] P. Barthelemy, J. Bertolotti, and D. S. Wiersma, Nature (London) **453**, 495 (2008).

[5] C. W. J. Beenakker, C. W. Groth, and A. R. Akhmerov, Phys. Rev. B **79**, 024204 (2009).

[6] R. Burioni, L. Caniparoli, and A. Vezzani, Phys. Rev. E **81**, 060101(R) (2010); R. Burioni, L. Caniparoli, S. Lepri, and A. Vezzani, *ibid.* **81**, 011127 (2010); A. Vezzani, R. Burioni, L. Caniparoli, and S. Lepri, Philos. Mag. **91**, 1987 (2011).

[7] R. Kutner and Ph. Maass, J. Phys. A **31**, 2603 (1998).

[8] M. Schulz, Phys. Lett. A **298**, 105 (2002); M. Schulz and P. Reineker, Chem. Phys. **284**, 331 (2002).

[9] P. Buonsante, R. Burioni, and A. Vezzani, Phys. Rev. E **84**, 021105 (2011).

[10] P. Barthelemy, J. Bertolotti, K. Vynck, S. Lepri, and D. S. Wiersma, Phys. Rev. E **82**, 011101 (2010).

[11] References [4,10] use a different relation $\beta = \alpha + d - 2$ between the exponents in Eqs. (2.1) and (2.2), because their ensembles of spheres or disks are constructed such that $n(r)r^{-1}dr$ [rather than $n(r)dr$] is the fraction with radii between r and $r + dr$. See J. Bertolotti, K. Vynck, L. Pattelli, P. Barthelemy, S. Lepri, and D. S. Wiersma, Adv. Funct. Mater. **20**, 965 (2010).

[12] E. Barkai, V. Fleurov, and J. Klafter, Phys. Rev. E **61**, 1164 (2000).

[13] A. Davis and A. Marshak, in *Fractal Frontiers*, edited by M. M. Novak and T. G. Dewey (World Scientific, Singapore, 1997).

[14] H. Larralde, F. Leyvraz, G. Martinez-Mekler, R. Rechtman, and S. Ruffo, Phys. Rev. E **58**, 4254 (1998).

[15] S. V. Buldyrev, S. Havlin, A. Ya. Kazakov, M. G. E. da Luz, E. P. Raposo, H. E. Stanley, and G. M. Viswanathan, Phys. Rev. E **64**, 041108 (2001); S. V. Buldyrev *et al.*, Physica A **302**, 148 (2001).

[16] R. N. Mantegna and H. E. Stanley, Phys. Rev. Lett. **73**, 2946 (1994).

[17] M. F. Shlesinger, Phys. Rev. Lett. **74**, 4959 (1995).